

Published in final edited form as:

Lasers Surg Med. 2011 September ; 43(7): 686–695. doi:10.1002/lsm.21113.

Novel Methods to Incorporate Photosensitizers Into Nanocarriers for Cancer Treatment by Photodynamic Therapy

Shouyan Wang, PhD¹, Wenzhe Fan, PhD¹, Gwangseong Kim, PhD¹, Hoe Jin Hah, PhD¹, Yong-Eun Koo Lee, PhD¹, Raoul Kopelman, PhD^{1,*}, Manivannan Ethirajan, PhD², Anurag Gupta, BS², Lalit N. Goswami, PhD², Paula Pera, MS², Janet Morgan, PhD², and Ravindra K. Pandey, PhD^{2,**}

¹Department of Chemistry, University of Michigan, Ann Arbor, Michigan 48109

²PDT Center and Department of Dermatology, Roswell Park Cancer Institute, Buffalo, New York 14263

Abstract

Objective—A hydrophobic photosensitizer, 2-[1-hexyloxyethyl]-2-devinyl pyropheophorbide-a (HPPH), was loaded into nontoxic biodegradable amine functionalized polyacrylamide (AFPAA) nanoparticles using three different methods (encapsulation, conjugation, and post-loading), forming a stable aqueous dispersion. Each formulation was characterized for physicochemical properties as well as for photodynamic performance so as to determine the most effective nanocarrier formulation containing HPPH for photodynamic therapy (PDT).

Materials and Methods—HPPH or HPPH-linked acrylamide was added into monomer mixture and polymerized in a microemulsion for encapsulation and conjugation, respectively. For post-loading, HPPH was added to an aqueous suspension of pre-formed nanoparticles. Those nanoparticles were tested for optical characteristics, dye loading, dye leaching, particle size, singlet oxygen production, dark toxicity, *in vitro* photodynamic cell killing, whole body fluorescence imaging and *in vivo* PDT.

Results—HPPH was successfully encapsulated, conjugated or post-loaded into the AFPAA nanoparticles. The resultant nanoparticles were spherical with a mean diameter of 29 ± 3 nm. The HPPH remained intact after entrapment and the HPPH leaching out of nanoparticles was negligible for all three formulations. The highest singlet oxygen production was achieved by the post-loaded formulation, which caused the highest phototoxicity in *in vitro* assays. No dark toxicity was observed. Post-loaded HPPH AFPAA nanoparticles were localized to tumors in a mouse colon carcinoma model, enabling fluorescence imaging, and producing a similar photodynamic tumor response to that of free HPPH in equivalent dose.

Conclusions—Post-loading is the promising method for loading nanoparticles with hydrophobic photosensitizers to achieve effective *in vitro* and *in vivo* PDT. *Lasers Surg. Med.* 43:686–695, 2011.

Keywords

HPPH; post-loading; polyacrylamide; biodegradable; photodynamic therapy; cancer treatment

INTRODUCTION

Cancer continues to be one of the world's most devastating categories of diseases with estimates of more than 12 million new cases every year [1]. Currently, the most common cancer treatments include surgical intervention, radiation, and chemotherapy. Unfortunately destruction of surrounding normal tissue, due to these treatments, kill and damage healthy cells, causing toxic side effects. Effective and less harmful alternatives to these classical therapies are persistently sought [2]. Photodynamic therapy (PDT), one such alternative is considered an innovative and attractive modality for treating localized and superficial tumors [3,4]. PDT utilizes the combined action of photosensitizers and specific light wavelengths for the treatment of various cancers. Following the activation of the photosensitizers by light, reactive oxygen species are generated from the prevailing molecular oxygen, mediating the destruction of cancer cells [3–5]. Important advantages of PDT over other therapies are that: (1) it is precisely targeted by selective illumination, (2) it can be repeated at the same site if needed, (3) it has low morbidity, and (4) it is much less invasive than surgery [4].

For successful PDT, the availability of suitable photosensitizers and an appropriate formulation are of crucial importance. Photofrin (porfimer sodium), one of the photosensitizers approved for cancer therapy in the United States, Europe, Japan, and Canada, causes cutaneous photosensitivity lasting 1–3 months [6]. Prolonged skin photosensitivity has also been reported for the second-generation photosensitizer Foscan (tetra [m-hydroxyphenyl]chlorin (mTHPC)) [6]. The new photosensitizer, 2-devinyl-2-(1-hexyloxyethyl) pyropheophorbide (HPPH) is a highly lipophilic drug with a log P (the logarithm of partition coefficient) of 5.6 at physiological pH [7]. Its large molar extinction coefficient in the red region of the visible spectrum ($\epsilon_{665\text{ nm}} \sim 47,500\text{ M}^{-1}\text{ cm}^{-1}$) and singlet oxygen quantum yield of 0.48 make it an attractive candidate for the PDT of malignant tumors [8–10]. HPPH, already used in several clinical trials [6,9,11–13] and currently in Phase I human clinical trials for Head and Neck cancer, shows only mild skin photosensitivity for a few days post PDT and elicits considerably less potential for cutaneous phototoxicity than in patients receiving Photofrin or Foscan [6].

PDT drugs in their free state need to be lipophilic to pass through cellular membranes and reach subcellular sites sensitive to the initial oxidative damage that will subsequently destroy cells. However, HPPH has poor solubility under physiological conditions, thus its formulation for intravenous delivery for *in vivo* PDT requires 1% Tween 80/5% dextrose formulation. Recent advances in nanochemistry offer exciting opportunities for the design and fabrication of a wide variety of delivery vehicles which enable a stable dispersion of lipophilic drugs into aqueous systems [14–17]. Nanoparticles are formulated from a range of biocompatible materials and can be engineered to carry an array of substances in a controlled and targeted manner. Upon systemic administration, such drug-doped carriers are preferentially taken up by tumor tissues by virtue of the “enhanced permeability and retention effect,” which is the tendency of such tissues to retain circulating macromolecules and particles owing to their “leaky” vasculature and poor drainage [18,19]. There are several delivery strategies known to stabilize PDT drugs in aqueous systems, such as liposomes, polymeric micelles, polymer nanoparticles, gold nanoparticles, and colloidal silica-based nanoparticles [17,20–30]. Most of the commonly used synthetic polymers employed to prepare nanoparticles for drug delivery are biodegradable [16].

It has been demonstrated that polyacrylamide (PAA) nanoparticles are promising vehicles for photodynamic drug delivery [25,26,29]. The PAA nanoparticle matrix, generally a porous hydrogel protects the embedded active form of photosensitizers from enzymatic or environmental degradation and permits molecular oxygen diffusion through the pores

[26,29]. Activation of the photosensitizer by light can lead to the formation of singlet oxygen, by energy transfer from the excited photosensitizer to the molecular oxygen, which can then diffuse out of the porous PAA matrix to produce a cytotoxic effect in tumor cells.

Studies on the biodistribution and excretion pathways of PAA nanoparticles following intravenous administration show that they are biodegradable and exhibit bi-exponential kinetics and differential excretion profiles which indicate that the clearance of the nanoparticles is biphasic with the greatest amount excreted in the first 24 hours [31]. Our previous work shows that photosensitizers encapsulated in PAA nanoparticles retain their PDT effectiveness, but loading of the reactive agent was low and thus relatively large amounts of nanoparticles were needed for significant cell kill [23–25,32].

Here we report on a nontoxic biodegradable nanocarrier, consisting of amine functionalized polyacrylamide nanoparticles, synthesized by a micro-emulsion polymerization method, for PDT drug delivery. Photosensitizer doped nanoparticles were prepared by encapsulation, conjugation, or post-loading to find the most efficient loading method for achieving high PDT efficiency. The singlet oxygen production efficiency of the formulations was tested in solution using a chemical probe [22,25,29] and *in vitro* cell kill and *in vivo* tumor response was compared.

MATERIALS AND METHODS

Chemicals

2-[1-hexyloxyethyl]-2-devinyl pyropheophorbide-a (HPPH) was synthesized as previously described [29,30]. All photophysical experiments were carried out using spectroscopic grade solvents. The reactions were monitored by thin-layer chromatography (TLC) and/or spectrophotometry. TLC was performed on ANALTECH pre-coated silica gel GF PE sheets (Cat. 159017, layer thickness 0.25 mm). Column chromatography was performed either over silica gel 60 (70–230 mesh) or neutral alumina (Brockmann grade III, 50 mesh). In some cases preparative TLC plates were used for purification (ANALTECH precoated silica gel GF glass plate, Cat. 02013, layer thickness 1.0 mm). Dichloromethane was dried over P₂O₅ under a N₂ atmosphere. The synthetic intermediates and the final products were characterized by NMR (400 MHz) and mass spectrometry (EIMS or HRMS). NMR spectra were recorded on a Bruker DRX 400 MHz spectrometer at 303 K in a CDCl₃ solution and referenced to residual CHCl₃ (7.26 ppm). EI-Mass spectra were run on a Bruker Esquire ion-trap mass spectrometer equipped with a pneumatically assisted electrospray ionization source, operating in positive mode. UV–visible spectra were recorded on a Varian Cary 50 Bio UV–Visible spectrophotometer using dichloromethane or methanol as the solvent.

In case of nanoparticle synthesis, acrylamide, *N,N,N',N'*-tetraethylmethylenediamine (TEMED), ammonium persulfate (APS), polyethylene glycol dodecyl ether (Brij 30), 3-(acryloyloxy)-2-hydroxypropyl methacrylate (AHM), *N*-ethyl-*N'*-(3-dimethylaminopropyl) carbodiimide hydrochloride, 4-dimethylamino pyridine, hexane, dimethyl sulfoxide (DMSO), and dioctyl sulfosuccinate (AOT) were purchased from Sigma Aldrich (St. Louis, MO, USA). 3-(aminopropyl) methacrylamide (APMA) was obtained from Polysciences Inc. (Warrington, PA, USA) and ethanol (190 proof) was obtained from Fisher Scientific (Suwanee, GA, USA). All solutions were prepared with 18 MΩ water purified by a Millipore Milli-Q Advantage A10 water purification system.

Preparation of Nanoparticles

Polymerization of blank biodegradable AFPAA nanoparticles—Hexane (45 ml) was added to a dry 100 ml round bottom flask and stirred under a constant purge of argon.

Suitable amounts of AOT (1.6 g) and Brij 30 (3.1 g) were added to the reaction flask and stirring was continued under argon protection for 20 minutes. Acrylamide (711 mg), APMA (89 mg), and biodegradable AHM (428 mg) were dissolved in phosphate buffered saline (2 ml) (PBS, 10 mM pH = 7.4) in a glass vial by sonication to obtain a uniform solution. The solution was then added to the hexane reaction mixture and vigorously stirred for another 20 minutes at room temperature. Polymerization was initiated by adding freshly prepared ammonium persulfate aqueous solution (10% w/v aqueous solution, 40 μ L) and TEMED (40 μ L). The resulting solution was stirred vigorously overnight. At the completion of polymerization, hexane was removed by rotary evaporation and the particles were precipitated by addition of ethanol (50 ml). The surfactant and residual monomers were washed away from the particles with ethanol (150 ml) followed by washing with water (100 ml) 5 times each in an Amicon ultra-filtration cell equipped with a Biomax 500 kDa cutoff membrane. The concentrated nanoparticles were lyophilized for two days for storage, and reconstituted by suspending in PBS before use.

HPPH encapsulated AFPAA nanoparticles—The polymerization procedures were the same except that HPPH (4.0 mg in 50 μ L DMSO) was added to the monomer mixture before injection into the solvent phase, and the production process was protected from light.

HPPH conjugated AFPAA nanoparticles—For the preparation of PS conjugated PAA NPs, the procedures as discussed above was followed by using the HPPH-modified monomer (5.0 mg) instead of HPPH, which was synthesized by following the reaction sequences depicted in Scheme 1.

Synthesis of HPPH-N-(3-aminopropyl) methylacrylamide—HPPH (50 mg, 0.078 mmol) was added to a dry round-bottomed flask and dissolved in dry dichloromethane (30.0 ml). To this, N-(3-Aminopropyl) methyl-acrylamide hydrochloride (20.9 mg, 0.117 mmol), *N*-Ethyl-*N'*-(3-dimethylaminopropyl) carbodiimide hydrochloride (30.0 mg, 0.157 mmol) and 4-dimethylamino pyridine (19.1 mg, 0.157 mmol) were added and the resultant mixture was stirred for 12 hours at room temperature under N₂ atmosphere. The reaction mixture was then diluted with dichloromethane (50 ml) and washed with brine (50 ml). The organic layer was separated, dried over sodium sulfate and concentrated. The product was purified over a silica gel column using 1–3% methanol-dichloromethane as mobile phase. Yield: 55.0 mg (91.9%); UV-vis λ_{\max} (in CH₂Cl₂): 661 nm (ϵ 5.3 \times 10⁴), 604 nm (ϵ 0.8 \times 10⁴), 537 nm (ϵ 1.0 \times 10⁴), 505 nm (ϵ 1.0 \times 10⁴), and 410 nm (ϵ 11.0 \times 10⁴); ¹H NMR (400 MHz, CDCl₃): δ 9.78 (singlet, 1H, meso-H), 9.38 (split singlet, 1H, meso-H), 8.52 (singlet, 1H, meso-H), 6.49 (m, 1H, NH), 5.92–5.86 (m, 2H, CH₃CHOhexyl & NH), 5.66 (s, 1H, –C=CHH), 5.29 (d, 1H, 15¹-CHH, *J* = 19.6 Hz), 5.26 (s, 1H, –C=CHH), 5.10 (d, 1H, 15¹-CHH, *J* = 19.6 Hz), 4.51 (q, 1H, 17-H, *J* = 6.4 Hz), 4.33 (d, 1H, H-18, *J* = 7.6 Hz), 3.68–3.62 (m, 4H, 8-CH₂CH₃ & –OCH₂-Hexyl), 3.50 (split singlet, 3H, ring-CH₃), 3.38 (singlet, 3H, ring-CH₃), 3.27 (singlet, 3H, ring-CH₃), 3.11–3.01 (m, 4H, –2NHCH₂), 2.67 (m, 1H, 17²-CHH), 2.42 (m, 1H, 17²-CHH), 2.31 (m, 1H, 17¹-CHH), 2.12 (d, 3H, CH₃CH-Ohexyl, *J* = 6.8 Hz), 2.03 (m, 1H, 17¹-CHH), 1.90 (s, 3H, CH₃-Acrylic chain), 1.81 (d, 3H, 18-CH₃, *J* = 6.0 Hz), 1.75 (t, 2H, CH₂-Acrylic chain, *J* = 8.4 Hz), 1.71 (t, 3H, 8-CH₂CH₃, *J* = 6.8 Hz), 1.40–1.36 (m, 4H, –2CH₂-Hexyl), 1.29–1.22 (m, 4H, –2CH₂-Hexyl), 0.80 (t, 3H, CH₃-Hexyl, *J* = 5.6 Hz), 0.49 (brs, 1H, NH), –1.56 (brs, 1H, NH). EIMS: 784 (M⁺ + Na). HRMS: calculated for C₄₆H₆₀N₆O₄: 760.4676. Found: 760.4153.

HPPH post-loaded AFPAA nanoparticles—Lyophilized blank AFPAA nanoparticles were suspended in 1% Tween 80 solution, 50 μ L of HPPH (20 mg/ml in DMSO) was added and the mixture was stirred at room temperature for at least 2 hours, followed by washing with PBS in an Amicon Ultra Centrifugal Filter Device (Amicon Ultra-15, 30 kDa filter

cutoff (Millipore, Billerica, MA, USA) for 20 minutes at 5,000g) to remove the DMSO and any unincorporated photosensitizer. The filtrate was measured spectrophotometrically to measure the unloaded HPPH. The retentate was brought up to the original volume with PBS and recentrifuged repeatedly until no absorbance signal was detected in the filtrate. The nanoparticles were reconstituted to the original volume, syringe filtered with a 0.2 µm filter and stored at 4°C for future use.

Characterization of the Nanoparticles

Size and dispersity—The particles were sized by dynamic light scattering (DLS, Delsa™ Nano, Beckman Coulter, Inc., Brea, CA, USA) and scanning electron microscope (SEM, Philips ESEM XL30).

Quantification of dye loading—A suitable amount of dye loaded nanoparticles was suspended in 1% Tween 80 in water solution to measure the UV–vis absorbance (Shimadzu UV-1601 UV–VIS Spectrometer, Shimadzu Scientific Instruments Inc, Columbia, MD, USA). The amount of photosensitizer loaded was calculated by the Beer–Lambert law. Fluorescence spectroscopy (FluoroMax-3, Jobin Yvon/SPEX Division, Instruments S. A. Inc., Edison, NJ, USA) was also conducted to verify photosensitizer integrity after entrapment.

Singlet oxygen production and efficiency—Generation of singlet oxygen on light activation of the photosensitizer in the different formulations was measured using a chemical probe disodium 9,10-anthracenedipropionic acid (ADPA) as a detector, and its decay rate constant as the relative singlet oxygen production rate, when tested at the same concentration of photosensitizer as described previously [22,25,29].

Dye leaching test—Photosensitizer loaded nanoparticles (50 mg) were suspended in 1% Tween 80 in water or 9% BSA in PBST (PBS containing 1% Tween 80) (2–2.5 ml) by sonication. After 2 hours incubation at 37°C, the nanoparticles were washed with 1% Tween 80 in water 5 times in an Amicon Stirred Cell equipped with a 100 KDa cutoff membrane. This enables any micellar HPPH, associated with the Tween 80 and not with the nanoparticles, to be removed. The absorbance of HPPH in the filtrates was monitored during the washing process.

In Vitro Studies: Comparative PDT

Colon26 cells were maintained in RPMI supplemented with 10% bovine calf serum, l-glutamine and antibiotics at 37°C, 5% CO₂, 95% air, and 100% humidity. For the phototoxicity assay, Colon26 cells were seeded in 96-well plates at a density of 5,000 cells/well. After overnight incubation at 37°C HPPH loaded nanoparticles were added at a range of concentrations and incubated at 37°C for 4 hours in the dark. The cells were washed with PBS, fresh growth medium was added, and the plates were irradiated with 0.25–1 J/cm² of broadband (400–750 nm) light at 3.2 mW/cm², from a halogen lamp source. Cells were incubated for an additional 48 hours and in the last 4 hours the MTT assay was performed to determine cell growth. Briefly, 20 µl of 4.0 mg/ml of 3-[4, 5-dimethylthiazol-2-yl]-2,5-diphenyltetrazoliumbromide (MTT) in PBS was added to the wells. After 4 hours incubation the medium was removed and 100 µl DMSO was added to solubilize the formazan crystals formed by cellular dehydrogenase activity. Absorbance was read on a microtiter plate reader at 550 nm. Experiments were performed 3 times. Cell growth after PDT was expressed relative to the growth of untreated controls.

In Vivo Studies

All animal work was performed under protocols preapproved by the Roswell Park Cancer Institute IACUC in accordance with the Guide for the Use of Laboratory Animals. Eight to twelve-week-old BALB/cAnNCr mice (Jackson Laboratory, Bar Harbor, ME) were inoculated intradermally on the shoulder with 1×10^6 Colon26 cells. When the tumor volume reached 40–70 mm³ based on the formula volume = length \times width²/2, they were injected *i.v.* via lateral tail vein with the therapeutic dose of photosensitizer diluted in D5W (0.47 μ mol/kg) in the form of HPPH or HPPH post-loaded AFPAA NPs. Before imaging and PDT, the area around the tumor was shaved and depilated with the depilatory cream Nair.

Planar fluorescence imaging of HPPH and HPPH post-loaded AFPAA NPs—

BALB/c mice in groups of three, were anesthetized with ketamine/xylazine (100/10 mg/kg *i.p.*) prior to imaging and imaged 24 hours post injection. Whole body fluorescence images were acquired with a 12 Bit monochrome Nuance CCD Camera (CRI, Woburn, MA). A continuous wave dye laser set to 665 nm was used to excite the photosensitizer and the fluorescence emission was collected beyond 695 nm with a 695 nm long-pass filter. The HPPH fluorescence intensity was measured in a region of interest located over the tumor, background due to autofluorescence in the control mouse was subtracted, and the mean and standard deviation of the three mice was calculated. The fluorescence images of control mice, HPPH and HPPH post-loaded PAA nanoparticles were scaled to the same range in ImageJ (NIH) for comparison.

In vivo PDT—BALB/c mice in groups of 10 were immobilized in plexi-glass holders 24 hours post *i.v.* injection and tumors were irradiated at 665 nm with a fluence of 135 J/cm² at a fluence rate of 75 mW/cm² using a pumped argon-dye laser. Mice were monitored for 60 days post PDT treatment for tumor regrowth. Tumors that regrew were measured with calipers three times per week until the volume reached the endpoint of >400 mm³, when the animals were euthanized.

RESULTS AND DISCUSSION

A major challenge in PDT is the preparation of suitable pharmaceutical formulations for lipophilic photosensitizers, which have inherently poor water solubility, and thus tend to aggregate under physiological conditions. Aggregated photosensitizers lose their photosensitizing activity because the singlet oxygen quantum yield is lower than the monomeric forms [33]. This may be ascribed to the fast radiation-less excitation energy relaxation that prevails within aggregates, due to interactions between photosensitizer molecules that shorten the lifetime of the excited state of the photosensitizer, thus reducing the probability of the molecule spin-converting to the triplet level, from which most photochemical processes start [34]. Embedding photosensitizers in AFPAA nanoparticles may prevent them from aggregating. In the encapsulation and conjugation methods the free photosensitizer or the photosensitizer-monomer conjugates mix with the polymer precursor solution and the hydrogel network formation and drug incorporation are accomplished simultaneously, maintaining the monomeric form of the photosensitizer. In the post-loading method, after the hydrogel networks are formed, maintenance of the original monomeric photosensitizer form occurs by the chargecharge or hydrophobic interactions between the hydrogel and the photosensitizer.

Figure 1a shows an SEM micrograph of as-prepared encapsulated nanoparticles. The blank, HPPH-conjugated and HPPH-post-loaded nanoparticles exhibited a similar size and morphology. The nanoparticles have a diameter of 29 ± 3 nm, with a fairly uniform size

distribution. The DLS measurements in aqueous solution (Fig. 1b) indicated good monodispersity (Polydispersity index = 0.111) of the AFPAA blank nanoparticles, but an average diameter of 39 nm. The difference may be attributed to swelling, which is typical for hydrogels [35–37].

Figure 2 and the inset show the UV–vis spectra of: 4.0 μM free HPPH (in 1% Tween 80 aqueous solution), blank AFPAA nanoparticles and dye loaded nanoparticles. The free HPPH has a strong absorbance peak at 665 nm. Importantly, blank AFPAA nanoparticles show minimal absorbance in the wavelength range studied, including the 600–900 nm range which is considered the useful therapeutic region for photodynamic therapy, due to the high tissue penetration of light at these wavelengths [22,38]. This ensures that AFPAA particles are suitable as drug carriers in photodynamic therapy. The spectral similarity between the free HPPH and the HPPH encapsulated or post-loaded nanoparticles in aqueous solutions, confirms that there are no chemical changes in HPPH after being entrapped inside the AFPAA nanoparticles, irrespective of the method of preparation. The HPPH conjugated nanoparticles show a strong absorbance peak near 662 nm, which is the same as that of the precursor used for conjugation (not shown). The HPPH loading per nanoparticle varies with the preparation method because of their different loading capacities. Based on the absorbance peak values and the extinction coefficient of HPPH in 1% Tween 80 solution, and relative to a nanoparticle concentration of 1.0 mg/ml, the post-loaded nanoparticles have the highest HPPH loading, 15.0 μM , followed by conjugated nanoparticles, 1.2 μM , and then encapsulated nanoparticles, 0.2 μM .

A similar order was observed for loading efficiency—defined as the percentage of the loaded amount of HPPH per nanoparticle with respect to the input amount of HPPH—that was 95%, 16%, and 4%, for the post-loaded, conjugated and encapsulated nanoparticles, respectively. Note that the spectra of HPPH encapsulated and conjugated AFPAA nanoparticles show slight light scattering phenomena (demonstrated by the broadening of the peak) in the therapeutic window, probably because of the relatively higher nanoparticle concentration than that of HPPH post-loaded nanoparticles. The greater drug loading and efficiency, and the ease of preparation of the post-loaded form compared to the other nanoparticles, indicates that post-loading is both a convenient and efficient way for loading a large amount of a hydrophobic photosensitizer into the AFPAA nanoparticle matrix.

Figure 3 presents the fluorescence emission spectra of 0.5 μM HPPH, and the as-prepared drug loaded nanoparticles in 1% Tween 80 in water solution, excited at 415 nm. All preparations demonstrated typical HPPH fluorescence spectra, indicating the photosensitizer was intact.

Photosensitizer Leaching

Anticipating *in vivo* applications, the nanoparticles were incubated in PBS containing 9% BSA, mimicking physiological condition, to determine the retention of HPPH in biological fluids. The nanoparticles were washed with 1% Tween 80 in PBS to prevent possible aggregation of HPPH in PBS. No HPPH was detectable in the filtrates of either the HPPH encapsulated or conjugated AFPAA nanoparticles, under these conditions. For HPPH post-loaded nanoparticles, HPPH did not leach into a 1% Tween 80 water solution presumably because they had a greater affinity for the hydrogel. In contrast, washing with 95% ethanol completely leached HPPH, which can be ascribed to the higher solubility of HPPH in the organic solvent and the precipitation of the AFPAA hydrogel in 95% ethanol. The amount of HPPH collected in all the filtrates after washing post-loaded AFPAA nanoparticles in the presence of 9% BSA PBST, amounted to approximately 0.2% of the loaded photosensitizer, thus indicating stable retention of HPPH under these conditions.

Singlet Oxygen Generation on Light Activation

Figure 4 shows the generation of singlet oxygen in HPPH post-loaded nanoparticles as an example. The relative rate constant for singlet oxygen production measured by the decay of ADPA was $1.51 \times 10^{-4}/s$ for free HPPH at 1.0 μM in 1% Tween 80 water. For HPPH at 1.0 μM entrapped in nanoparticles, the relative rate constants were $0.48 \times 10^{-4}/s$ for HPPH encapsulated in nanoparticles at 5.0 mg/ml, $1.23 \times 10^{-4}/s$ for HPPH conjugated nanoparticles at 1.0 mg/ml, and $1.41 \times 10^{-4}/s$ for post-loaded nanoparticles at 0.067 mg/ml (Fig. 4). Thus singlet oxygen production efficiency is approximately 32%, 81%, and 93%, compared to the free HPPH drug, for encapsulated, conjugated and post-loaded nanoparticles, respectively. These results again indicate that the HPPH is intact after post-loading without serious degree of aggregation. Furthermore, the singlet oxygen produced is free to diffuse out of the hydrogel nanoparticles and react with the ADPA [22].

In Vitro PDT

The phototoxicity assay (Fig. 5) demonstrates that, for equivalent molar doses of HPPH in the AFPAA nanoparticles, the post-loaded formulation was the most effective at inducing phototoxicity. A comparative study of HPPH post-loaded in PAA NPs with free HPPH did not show any significant difference in photosensitizing efficacy. However, the HPPH encapsulated form, or conjugated inside the PAA NPs produced less phototoxicity. No significant dark toxicity was observed with all formulations.

Planar Fluorescence Imaging

Among the nanoparticle formulations, HPPH post-loaded AFPAA nanoparticles provided the best PDT response in Colon26 cells. Therefore the accumulation of HPPH post-loaded AFPAA nanoparticles was compared with free HPPH in tumors *in vivo* by whole body fluorescence imaging of BALB/c mice bearing Colon26 tumors. The imaging was performed 24 hours post *i.v.* injection, the time at which maximum accumulation of free HPPH within the tumor is found. Figure 6 shows that the average fluorescence intensity of HPPH post-loaded nanoparticles is slightly higher ($1,984 \pm 657$) than that of HPPH alone ($1,359 \pm 671$) at the therapeutic dose for free HPPH (0.47 $\mu mol/kg$), but the difference is not significant ($P > 0.05$, 2-tailed *t*-test, $n = 3$). This indicates that the nanoparticles are capable of delivering HPPH to the site of the tumor.

In Vivo PDT

The *in vivo* PDT efficacy of the HPPH post-loaded AFPAA nanoparticles was next compared to free HPPH in BALB/c mice bearing Colon26 tumors. The tumor response was 40% for both groups as shown in Figure 7. A similar tumor response was expected since the estimated HPPH in the tumors was not significantly different based on the fluorescence imaging data. It is possible that the pharmacokinetic properties of free HPPH may vary in its PAA NPs formulation. Therefore, it is important to investigate the *in vivo* PDT efficacy of HPPH-PAA NPs formulation in larger group of mice at different drug/light doses and variable time intervals, and these studies are currently in progress.

Most of the porphyrin-based compounds are insoluble in water and the selection of an appropriate formulation suitable for *in vitro* and *in vivo* studies is extremely important. The PAA NPs due to its biodegradability and non-toxic nature provide great opportunity in formulating hydrophobic photosensitizers. In a parallel study, we have shown the utility of these nanoparticles in developing “Multifunctional” nanoplatforms for both imaging and therapy, which are otherwise difficult to synthesize. The PAA NPs also provide a platform

for developing improved/targeted nanoparticles by incorporating desired targeting moieties at the periphery of the nanoparticles, and these studies are currently underway.

CONCLUSIONS

Amine functionalized polyacrylamide nanoparticles were polymerized in a micro-emulsion. The particles were spherical with a mean diameter of 29 ± 3 nm. The hydrophobic photosensitizer HPPH was successfully encapsulated, conjugated or post-loaded into the AFPAA nanoparticles. The absorbance and fluorescence spectra confirmed that the HPPH was intact after being entrapped into the nanoparticles. HPPH was retained well by the nanoparticles with no leaching for encapsulated or conjugated nanoparticles, and minimal (0.2%) leaching for the post-loaded formulation in 9% BSA PBST solution. Singlet oxygen measurements showed that the post-loaded nanoparticles, which have the highest amount of HPPH per nanoparticle among the three formulations, have the highest photoreaction rate, with the efficiency of singlet oxygen production being 93%, relative to the same concentration of free HPPH. The photosensitizer loading efficiency was greatest (95%) by the post-loading method. Singlet oxygen production and loading efficiencies were much lower for conjugated nanoparticles, and lowest for encapsulated nanoparticles. *In vitro* experiments confirmed that there is no dark toxicity for all formulations. Importantly, the entrapped drug is able to generate singlet oxygen upon light irradiation, which resulted in irreversible destruction of cells. Whole body planar fluorescence imaging confirmed that HPPH post-loaded AFPAA nanoparticles are capable of delivering the photosensitizer to the tumor site, and PDT induced a similar tumor response to the free photosensitizer for an equivalent dose. Post-loading is thus a promising method for loading AFPAA nanoparticles with hydrophobic photosensitizers, which is effective for both *in vitro* and *in vivo* PDT. The presence of amine groups on the surface of the nanoparticles, allows further modifications to be made with molecules that can bind to biomarkers on the surface of cancer cells. Such nanoparticles could target cancer cells, resulting in more specific damage.

Acknowledgments

The Electron Microbeam Analysis Laboratory at the University of Michigan is also gratefully acknowledged for the use of the SEM.

Contract grant sponsor: NIH/NCI (R. Kopelman); Contract grant number: R33CA125297; Contract grant sponsor: NCI/NIH Nanoplatform Grant; Contract grant number: CA 119358; Contract grant sponsor: RPCI Cancer Center; Contract grant numbers: P30CA16056, R33CA125297, R33CA125297-03s1.

REFERENCES

1. Jemal A, Bray F, Center MM, Ferlay J, Ward E, Forman D. Global cancer statistics. *CA Cancer J Clin.* 2011; 61:69–90. [PubMed: 21296855]
2. Peer D, Karp JM, Hong S, Farokhzad OC, Margalit R, Langer R. Nanocarriers as an emerging platform for cancer therapy. *Nat Nanotechnol.* 2007; 2:751–760. [PubMed: 18654426]
3. Fayter D, Corbett M, Heirs M, Fox D, Eastwood A. A systematic review of photodynamic therapy in the treatment of precancerous skin conditions, Barrett's oesophagus and cancers of the biliary tract, brain, head and neck, lung, oesophagus and skin. *Health Technol Assess.* 2010; 14:1–288. [PubMed: 20663420]
4. O'Connor AE, Gallagher WM, Byrne AT. Porphyrin and nonporphyrin in oncology: Preclinical and clinical advances in photodynamic therapy. *Photochem Photobiol.* 2009; 85:1053–1074. [PubMed: 19682322]
5. Henderson BW, Gollnick SO, Snyder JW, Busch TM, Kousis PC, Cheney RT, Morgan J. Choice of oxygen-conserving treatment regimen determines the inflammatory response and outcome of photodynamic therapy of tumors. *Cancer Res.* 2004; 64:2120–2126. [PubMed: 15026352]

6. Bellnier DA, Greco WR, Nava H, Loewen GM, Oseroff AR, Dougherty TJ. Mild skin photosensitivity in cancer patients following injection of Photochlor (2-[1-hexyloxyethyl]-2-devinyl pyropheophorbide-a; HPPH) for photodynamic therapy. *Cancer Chemother Pharmacol.* 2006; 57:40–45. [PubMed: 16001178]
7. Henderson BW, Bellnier DA, Greco WR, Sharma A, Pandey RK, Vaughan LA, Weishaupt KR, Dougherty TJ. An in vivo quantitative structure-activity relationship for a congeneric series of pyropheophorbide derivatives as photosensitizers for photodynamic therapy. *Cancer Res.* 1997; 57:4000. [PubMed: 9307285]
8. Pandey RK, Sumlin AB, Constantine S, Aoudia M, Potter WR, Bellnier DA, Henderson BW, Rodgers MA, Smith KM, Dougherty TJ. Alkyl ether analogs of chlorophyll-a derivatives: Part 1. Synthesis, photophysical properties and photodynamic efficacy. *Photochem Photobiol.* 1996; 64:194–204. [PubMed: 8787014]
9. Bellnier DA, Greco WR, Loewen GM, Nava H, Oseroff AR, Pandey RK, Tsuchida T, Dougherty TJ. Population pharmacokinetics of the photodynamic therapy agent 2-[1-hexyloxyethyl]-2-devinyl pyropheophorbide-a in cancer patients. *Cancer Res.* 2003; 63:1806–1813. [PubMed: 12702566]
10. Furukawa K, Yamamoto H, Crean DH, Kato H, Mang TS. Localization and treatment of transformed tissues using the photodynamic sensitizer 2-[1-hexyloxyethyl]-2-devinyl pyropheophorbide-a. *Lasers Surg Med.* 1996; 18:157–166. [PubMed: 8833284]
11. Anderson TR, Dougherty TJ, Tan D, Sumlin A, Schlossin JM, Kanter PM. Photodynamic therapy for sarcoma pulmonary metastases. *Anticancer Res.* 2003; 23:3713–3718. [PubMed: 14666668]
12. Loewen G, Pandey R, Belliner D, Henderson B, Dougherty T. Endobronchial photodynamic therapy for lung cancer. *Lasers Surg Med.* 2006; 38:364–370. [PubMed: 16788932]
13. Sunar U, Rohrbach D, Rigual N, Tracy E, Keymel K, Cooper MT, Baumann H, Henderson BW. Monitoring photobleaching and hemodynamic responses to HPPH-mediated photodynamic therapy of head and neck cancer: A case report. *Opt Express.* 2010; 18:14969–14978. [PubMed: 20639983]
14. Baba K, Pudavar HE, Roy I, Ohulchanskyy TY, Chen YH, Pandey RK, Prasad PN. New method for delivering a hydrophobic drug for photodynamic therapy using pure nanocrystal form of the drug. *Mol Pharm.* 2007; 4:289–297. [PubMed: 17266331]
15. Wong J, Brugger A, Khare A, Chaubal M, Papadopoulos P, Rabinow B, Kipp J, Ning J. Suspensions for intravenous (IV) injection: A review of development, preclinical and clinical aspects. *Adv Drug Deliv Rev.* 2008; 60:939–954. [PubMed: 18343527]
16. Koo YEL, Reddy GR, Bhojani M, Schneider R, Philbert MA, Rehemtulla A, Ross BD, Kopelman R. Brain cancer diagnosis and therapy with nanoplateforms. *Adv Drug Deliv Rev.* 2006; 58:1556–1577. [PubMed: 17107738]
17. Cinteza LO, Ohulchanskyy TY, Sahoo Y, Bergey EJ, Pandey RK, Prasad PN. Diacyllipid micelle-based nanocarrier for magnetically guided delivery of drugs in photodynamic therapy. *Mol Pharm.* 2006; 3:415–423. [PubMed: 16889435]
18. Matsumura Y, Maeda H. A new concept for macromolecular therapeutics in cancer chemotherapy-mechanism of tumorotropic accumulation of proteins and the antitumor agent smancs. *Cancer Res.* 1986; 46:6387–6392. [PubMed: 2946403]
19. Maeda H. The enhanced permeability and retention (epr) effect in tumor vasculature: the key role of tumor-selective macromolecular drug targeting. *Advan Enzyme Regul.* 2001; 41:189–207. [PubMed: 11384745]
20. Cheng Y, Samia AC, Meyers JD, Panagopoulos I, Fei BW, Burda C. Highly efficient drug delivery with gold nanoparticle vectors for in vivo photodynamic therapy of cancer. *J Am Chem Soc.* 2008; 130:10643–10647. [PubMed: 18642918]
21. Yan F, Kopelman R. The embedding of meta-tetra(hydroxyphenyl)-chlorin into silica nanoparticle platforms for photodynamic therapy and their singlet oxygen production and pH-dependent optical properties. *Photochem Photobiol.* 2003; 78:587–591. [PubMed: 14743867]
22. Roy I, Ohulchanskyy TY, Pudavar HE, Bergey EJ, Oseroff AR, Morgan J, Dougherty TJ, Prasad PN. Ceramic-based nanoparticles entrapping water-insoluble photosensitizing anticancer drugs: A novel drug-carrier system for photodynamic therapy. *J Am Chem Soc.* 2003; 125:7860–7865. [PubMed: 12823004]

23. Gao D, Agayan RR, Xu H, Philbert MA, Kopelman R. Nanoparticles for two-photon photodynamic therapy in living cells. *Nano Lett.* 2006; 6:2383–2386. [PubMed: 17090062]
24. Gao D, Xu H, Philbert MA, Kopelman R. Ultrafine hydrogel nanoparticles: synthetic approach and therapeutic application in living cells. *Ange Chem Int Ed.* 2007; 46:2224–2227.
25. Tang W, Xu H, Kopelman R, Philbert MA. Photodynamic characterization and in vitro application of methylene blue-containing nanoparticle platforms. *Photochem Photobiol.* 2005; 81:242–249. [PubMed: 15595888]
26. Tang W, Xu H, Park EJ, Philbert MA, Kopelman R. Encapsulation of methylene blue in polyacrylamide nanoparticle platforms protects its photodynamic effectiveness. *Biochem Biophys Res Commun.* 2008; 369:579–583. [PubMed: 18298950]
27. Kim S, Ohulchanskyy TY, Pudavar HE, Pandey RK, Prasad PN. Organically modified silica nanoparticles co-encapsulating photosensitizing drug and aggregation-enhanced two-photon absorbing fluorescent dye aggregates for two-photon photodynamic therapy. *J Am Chem Soc.* 2007; 129:2669–2675. [PubMed: 17288423]
28. Vargas A, Eid M, Fanchaouy M, Gurny R, Delie F. In vivo photodynamic activity of photosensitizer-loaded nanoparticles: formulation properties, administration parameters and biological issues involved in PDT outcome. *Eur J Pharm Biopharm.* 2008; 69:43–53. [PubMed: 18023564]
29. Moreno MJ, Monson E, Reddy RG, Rehemtulla A, Ross BD, Philbert M, Schneider RJ, Kopelman R. Production of singlet oxygen by Ru(dpp(SO₃)(2))(3) incorporated in polyacrylamide PEBBLES. *Sens Actuator B Chem.* 2003; 90:82–89.
30. Harrell JA, Kopelman R. Biocompatible probes measure intracellular activity. *Biophoton Int.* 2000; 7:22.
31. Wenger Y, Schneider IIRJ, Reddy GR, Kopelman R, Joliet O, Philbert MA. Tissue distribution and pharmacokinetics of stable polyacrylamide nanoparticles following intravenous injection in the rat. *Toxicol Appl Pharmacol.* 2011; 251:181–190. [PubMed: 21134391]
32. Reddy GR, Bhojani MS, McConville P, Moody J, Moffat BA, Hall DE, Kim G, Koo YEL, Woolliscroft MJ, Sugai JV, Johnson TD, Philbert MA, Kopelman R, Rehemtulla A, Ross BD. Vascular targeted nanoparticles for imaging and treatment of brain tumors. *Clin Cancer Res.* 2006; 12:6677–6686. [PubMed: 17121886]
33. Lambert CR, Reddi E, Spikes JD, Rodgers MAJ, Jori G. The effects of porphyrin structure and aggregation state on photosensitized processes in aqueous and micellar media. *Photochem Photobiol.* 1986; 44:595–601. [PubMed: 3809256]
34. Kelbaskas L, Dietel W. Internalization of aggregated photosensitizers by tumor cells: subcellular time-resolved fluorescence spectroscopy on derivatives of pyropheophorbide-a ethers and chlorin e6 under femtosecond one- and two-photon excitations. *Photochem Photobiol.* 2002; 76:686–694. [PubMed: 12511052]
35. Zhang Y, Zhu W, Wang BB, Ding JD. A novel microgel and associated post-fabrication encapsulation technique of proteins. *J Controlled Release.* 2005; 105:260.
36. Chiu HC, Lin YF, Hung SH. Equilibrium swelling of copolymerized acrylic acid — Methacrylated dextran networks: Effects of pH and neutral salt. *Macromolecules.* 2002; 35:5235–5242.
37. Tan HP, Chu CR, Payne KA, Marra KG. Injectable in situ forming biodegradable chitosan-hyaluronic acid based hydrogels for cartilage tissue engineering. *Biomaterials.* 2009; 30:2499–2506. [PubMed: 19167750]
38. Pallenberg AJ, Dobhal MP, Pandey RK. Efficient synthesis of pyropheophorbide-a and its derivatives. *Org Proc Res Dev.* 2004; 8:287–290.

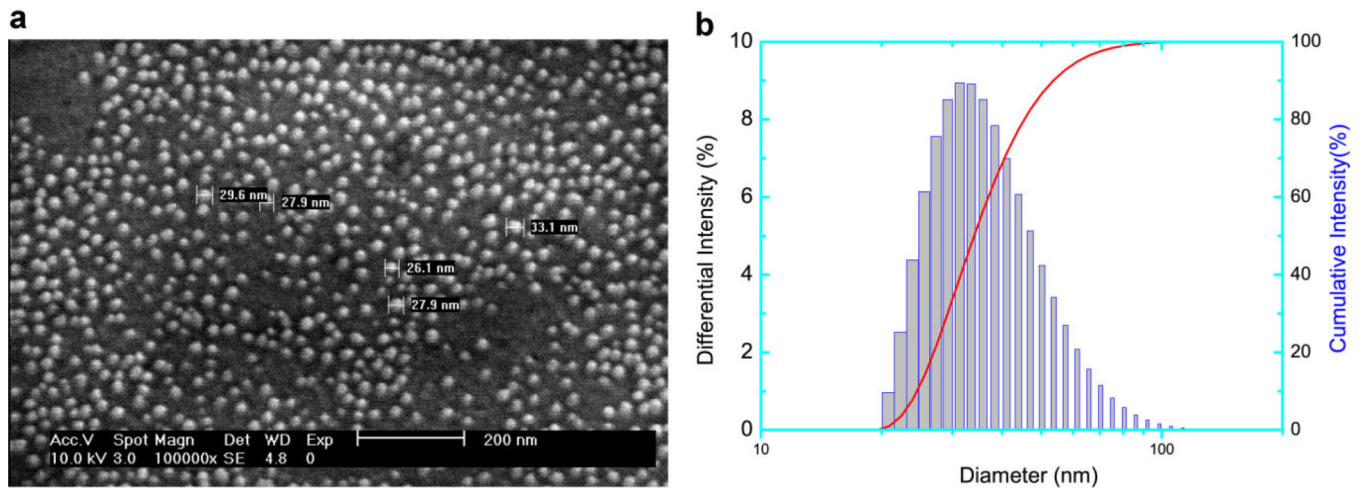


Fig. 1. SEM micrograph (a) and DLS (b) of as-synthesized HPPH encapsulated AFPAA nanoparticles.

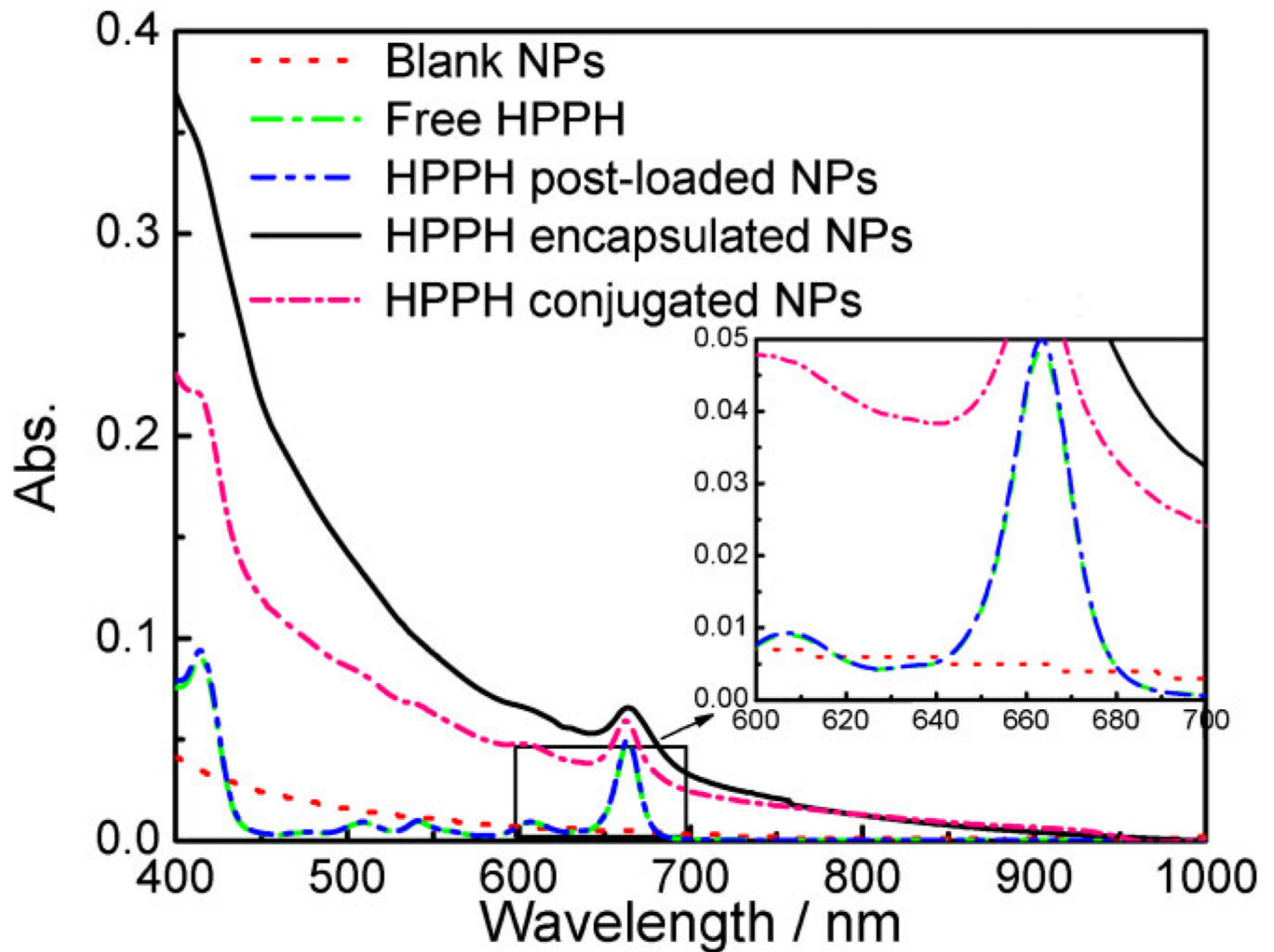


Fig. 2. UV-vis spectra of blank AFPAA nanoparticles (1.0 mg/ml in 1% Tween 80 in water solution, red dotted line), free HPPH (1.0 μ M, same as below, green dashed line), HPPH encapsulated AFPAA nanoparticles (5 mg/ml, black solid line, 1.0 μ M of HPPH), HPPH conjugated AFPAA nanoparticles (1.0 mg/ml, pink short dash dotted line, 1.0 μ M of HPPH) and HPPH post-loaded AFPAA nanoparticles (0.067 mg/ml, blue dash dotted line, 1.0 μ M of HPPH). Inset: Enlarged spectra in the 600–700 nm range.

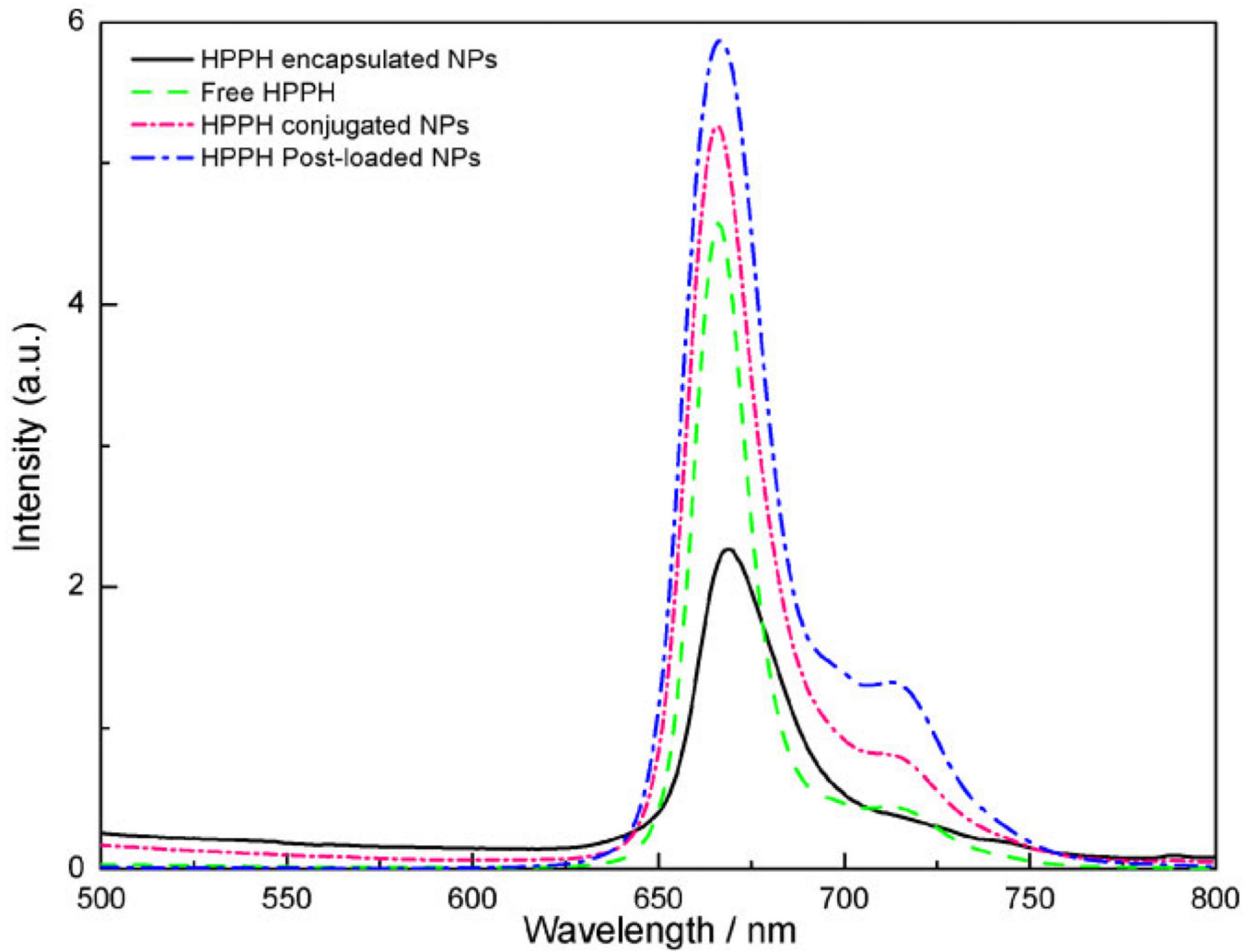


Fig. 3. Fluorescence emission spectra of free HPPH (0.5 μ M, green dashed line), HPPH encapsulated (2.5 mg/ml, black solid line, 0.5 μ M of HPPH), HPPH conjugated AFPAA nanoparticles (0.5 mg/ml, pink short dash dotted line, 0.5 μ M of HPPH) and HPPH post-loaded AFPAA nanoparticles (0.033 mg/ml, blue dash dotted line, 0.5 μ M of HPPH), all excited at 415 nm in 1% Tween 80. The arrows indicate the corresponding axes.

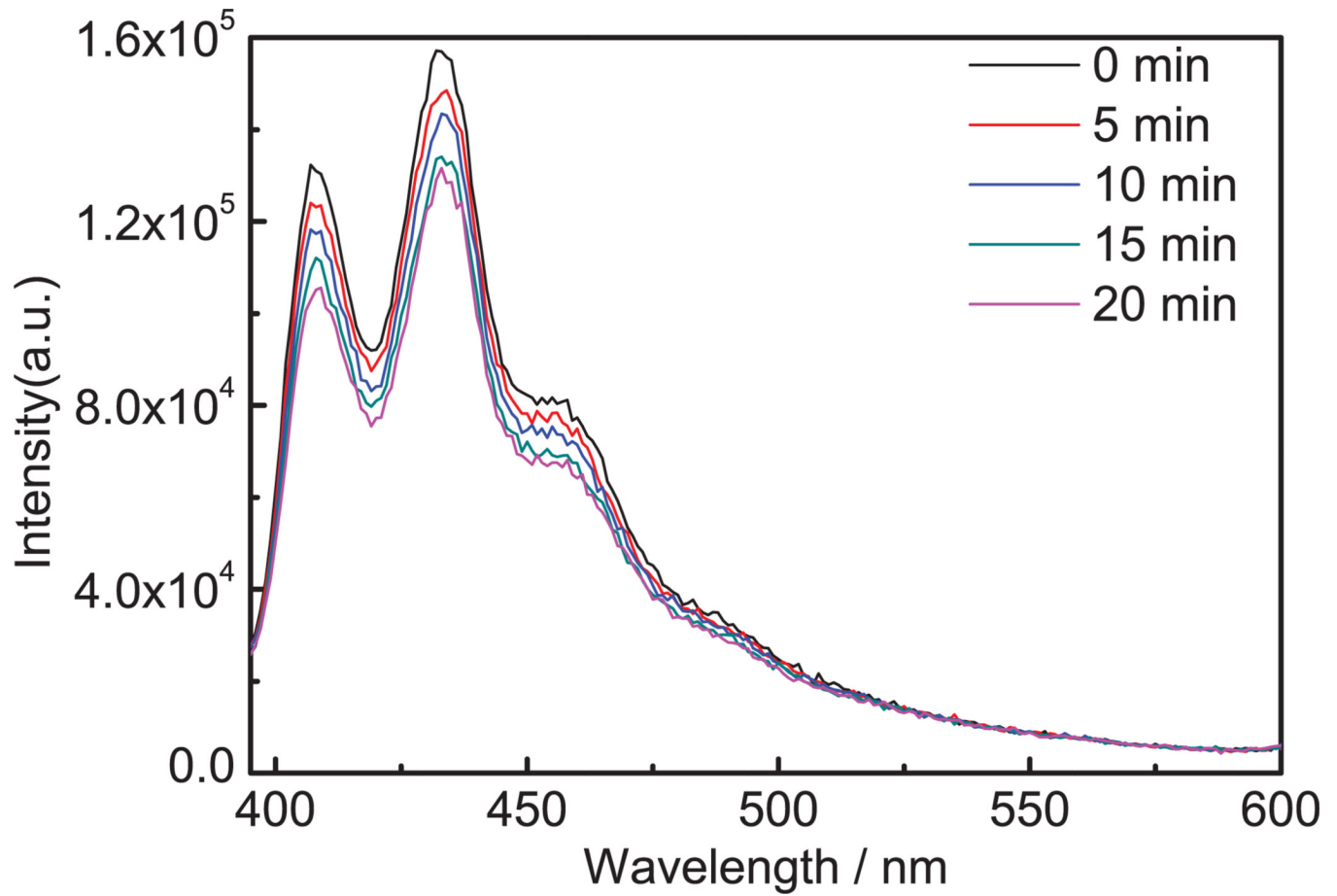


Fig. 4. Spectra of ADPA from a mixture of ADPA (4 μM) and HPPH post-loaded nanoparticles (0.067 mg/ml) illuminated at 665 nm for 0, 5, 10, and 20 minutes. The excitation slit was 10 nm and the emission slit was 2 nm.

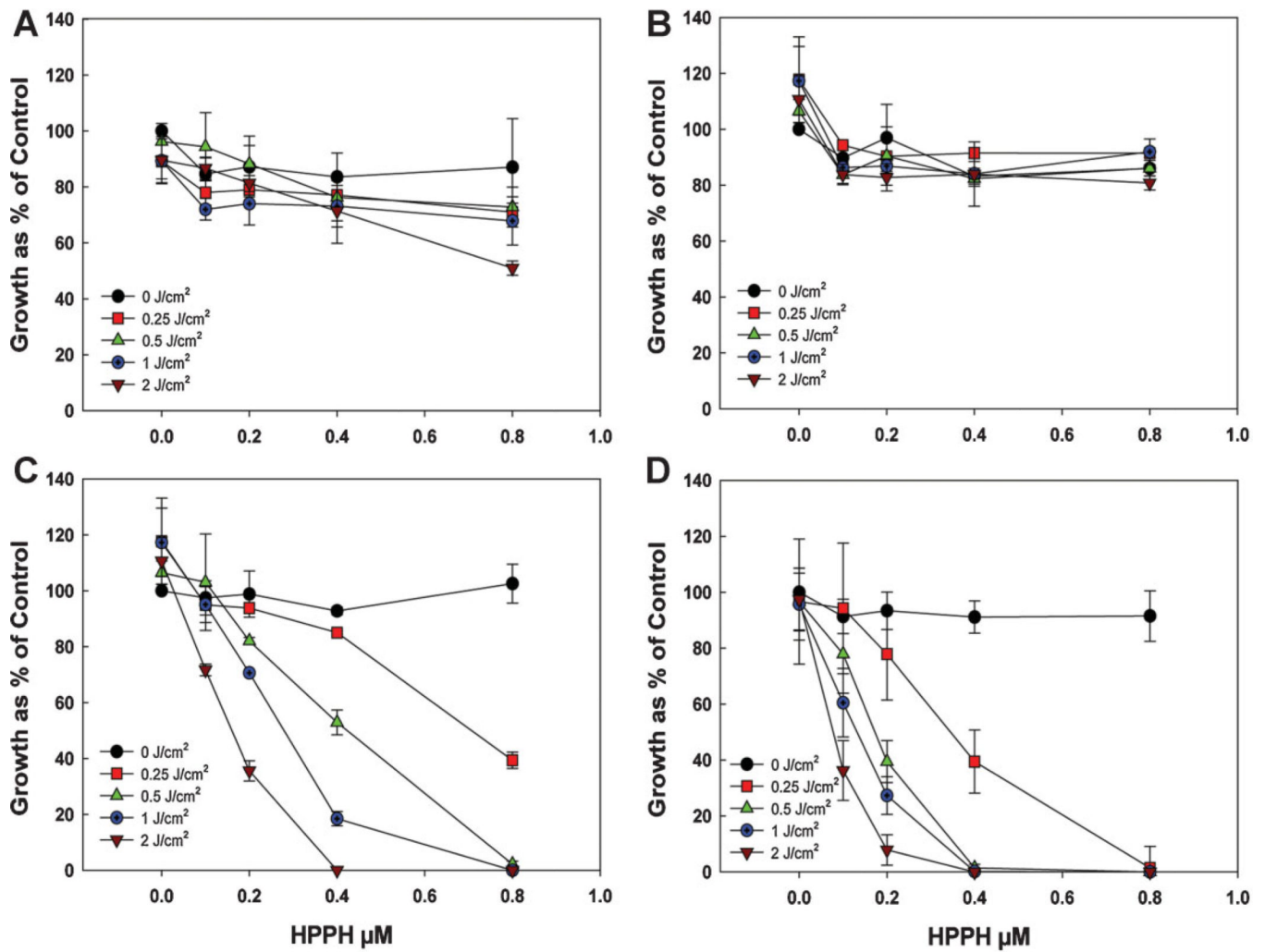


Fig. 5. Phototoxicity of Colon26 cells after incubation with the different preparations of AFPAA nanoparticles for 4 hours followed by light at a series of doses at a fluence rate of $3.2 \text{ mW}/\text{cm}^2$. Growth was assayed by the MTT method. (A) Encapsulated HPPH (PAA-E), (B) Conjugated HPPH (PAA-CONJ), (C) Post-loaded HPPH (PAA-PL), (D) Free HPPH. Values are the mean \pm standard deviation of 3–4 experiments.

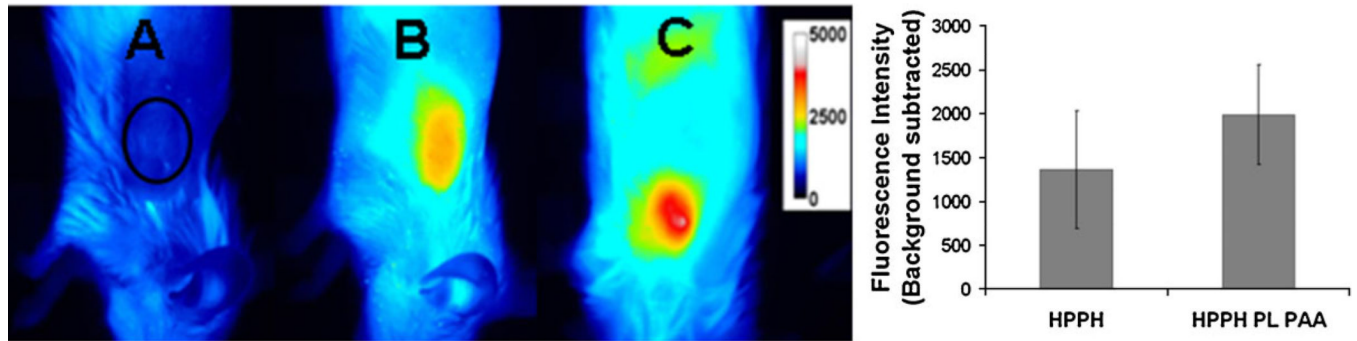


Fig. 6. Fluorescence optical imaging of BALB/c mice bearing Colon26 tumors. (A) Control mouse, no drug, black circle indicates location of tumor (B) 24 hours post-injection of HPPH (0.47 $\mu\text{mol/kg}$) and (C) 24 hours post-injection of HPPH post-loaded PAA nanoparticles (0.47 $\mu\text{mol/kg}$). The false-colored images are scaled to the same intensity range and show representative images with fluorescence intensity closest to the average values. The ROI over the tumor for measuring fluorescence intensity is indicated in A. The bar graph shows the fluorescence intensity in the ROI (average \pm standard deviation of three samples).

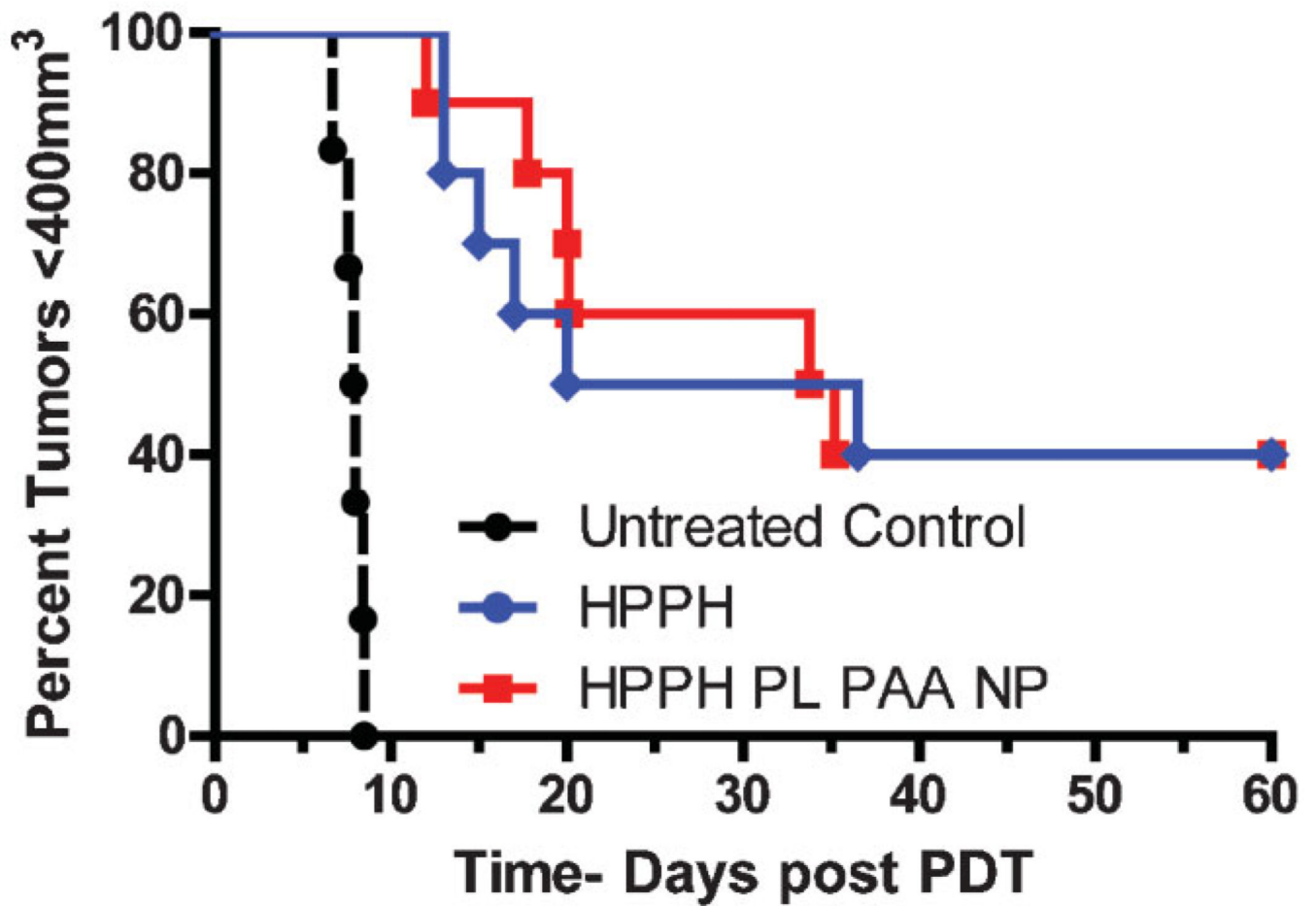
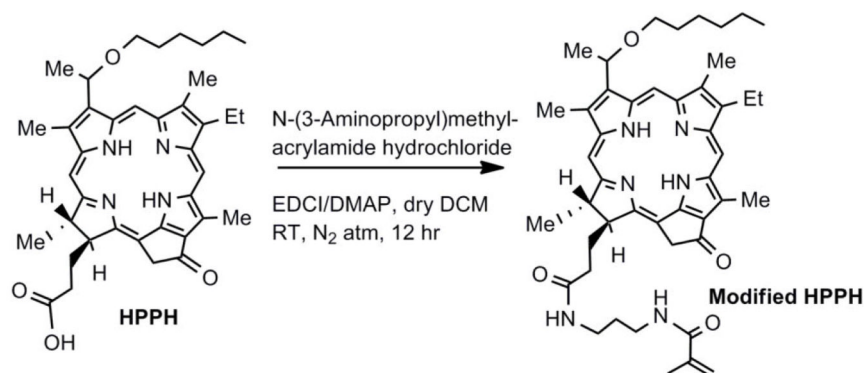
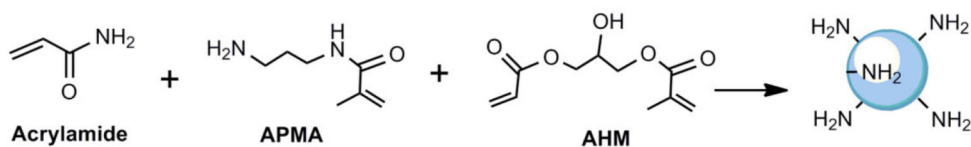
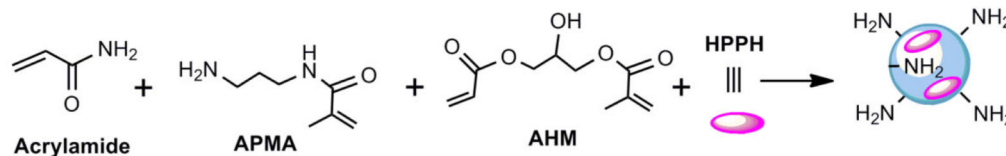
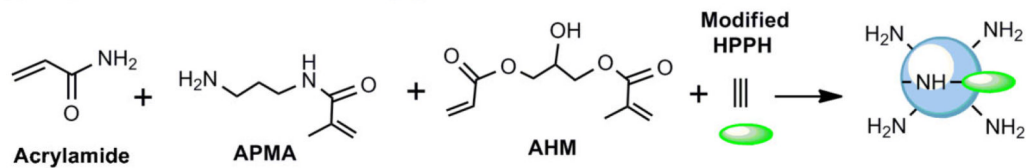


Fig. 7. Kaplan–Meier plots for BALB/c mice bearing Colon-26 tumors (10 mice/group). Treatment parameters: Photosensitizer dose: 0.47 $\mu\text{mol/kg}$, irradiation was at 665 nm, and the fluence was 135 J/cm^2 at a fluence rate of 75 mW/cm^2 .

A Preparation of modified HPPH**B Preparation of PAA nanoparticles****C Preparation of HPPH encapsulated PAA Nanoparticles****D Preparation of HPPH - PAA NP conjugate:****E Preparation of HPPH post-loaded PAA Nanoparticles****Scheme 1.**

Preparation of modified HPPH, blank PAA NPs, and the corresponding nanoformulations.